Imaging Cells and Tissues with Refractive Index Radiology

Y. Hwu,* W. L. Tsai,* H. M. Chang,† H. I. Yeh,‡ P. C. Hsu,* Y. C. Yang,* Y. T. Su,* H. L. Tsai,† G. M. Chow,§ P. C. Ho,¶ S. C. Li,¶ H. O. Moser,‖ P. Yang,‖ S. K. Seol,** C. C. Kim,** J. H. Je,** E. Stefanekova,†† A. Groso,†† and G. Margaritondo††

*Institute of Physics, Academia Sinica, Nankang, Taipei, Taiwan; †Pandis Biomedical Research Association, Chupei, Taiwan; ‡Departments of Medical Research and Internal Medicine, Mackay Memorial Hospital, Mackay Medicine, Nursing and Management College, and Taipei Medical University, Taipei, Taiwan; §Department of Materials Science and Singapore-Massachusetts Institute of Technology Alliance, National University of Singapore, Singapore; ¶Department of Pharmacy, National University of Singapore, Singapore; ‖Singapore Synchrotron Light Source, National University of Singapore, Singapore; **Department of Materials Science and Engineering, Pohang University of Science and Technology, Pohang, Korea; and ††Faculté des Sciences de Base, Ecole Polytechnique Fédérale, CH-1015 Lausanne, Switzerland

ABSTRACT Can individual cells, including live cells, be imaged using hard x rays? Common wisdom until now required sophisticated staining techniques for this task. We show instead that individual cells and cell details can be detected in culture solution and tissues with no staining and no other contrast-enhancing preparation. The sample examined can be much thicker than for many other microscopy techniques without sacrificing the capability to resolve cells. The key factor in our approach is the use of a coherent synchrotron source and of contrast mechanisms based on the refractive index. The first successful tests were conducted on a variety of cell systems including skin and internal leaf cells, mouse neurons, rabbit fibroblast cells, and human tumor cells.

INTRODUCTION

We present experimental evidence that synchrotron hard x rays are suitable for radiological imaging of thick and live biological samples down to the cellular level. In recent years, substantial research efforts drastically improved the lateral resolution and enhanced the contrast in synchrotron-based radiology (Hwu et al., 2002). In principle, radiological images based on hard x ray (wavelength <1 Å) achieved sufficient lateral resolution (Yun et al., 1999) and can resolve structures of biological samples down to the cell level. However, such performances have not been demonstrated without sophisticated staining procedures excluding live cells (Yun, 2004).

Cells can be observed in soft-x-ray microscopy using x rays with wavelengths in the so-called ''water window'' (284–543 eV) that maximizes the contrast between carbon-containing areas and water (Kirz et al., 1994; Jacobsen et al., 2002). The development of advanced x-ray optics successfully achieved the observation of subcell structures in hydrated state (Larabell et al., 2000; Ford et al., 2000; Weiß et al., 2000). However, x rays in this photon energy range cannot penetrate specimens thicker than a few tens of a micrometer, approximately the thickness of a single cell, and this limits their potential application. Moreover, there is no report that this type of approach can produce images of living cells due to the sample preparation requirements.

The key to our success in using hard x rays to image unstained cells was contrast based on the refractive index (Hwu et al., 2002). This enhanced the visibility of the edges between regions with different refractive index. As a result, fine details could be observed at the cellular and subcellular level without any staining or contrast-enhancing cell preparation.

This is an interesting complementary approach to the standard optical microscopy of living cells. In fact, x-ray microradiology has the capability to examine thicker samples in a more ''realistic'' environment and potentially even in living bodies. We demonstrate in this work, for example, that cellular detail within a sample as thick as 5 mm can still be clearly identified at selective depth from the sample surface without sacrificing the lateral resolution. Furthermore, recent tests based on advances in detectors and in image reconstruction demonstrated that the short wavelength of hard x rays can yield reconstructed images with 10–50-nm resolution—well beyond the diffraction limit of optical microscopy (Miao et al., 2002).

Edge enhancement cannot be easily observed with conventional x-ray sources due to their large size and angular spread (Hwu et al., 2002). In fact, the enhancement is due to small deviations of the x rays propagating through the edge, which is a region with high refractive-index gradient. A large source size and angular spread wash out the effect. To reduce this problem, one can either use an aperture to limit the effective source size or increase the source-sample distance. However, this greatly reduces the portion of the emitted x rays that is actually used for radiological imaging.

Synchrotron sources remove the problem because of their natural coherence (Hwu et al., 2002; Margaritondo, 2002). The x rays are emitted from a small source area and are strongly collimated. Edge enhancement thus becomes easily

Submitted October 2, 2003, and accepted for publication September 14, 2004.

Address reprint requests to J. H. Je, E-mail: jhje@postech.ac.kr.

0006-3495/04/12/4180/08 $2.00

doi: 10.1529/biophysj.103.034991

visible and—as we demonstrate here—microradiology of live cells is feasible. Our experimental results show indeed that fine details can be imaged with high lateral and time resolution in a variety of biology materials. These included leaf skin cells, human tumor cells, mouse neurons, and rabbit bone cells.

Fig. 1 shows a nice example of our results: the image of a *Xenopus* oocyte. Note that one can clearly identify the animal pole (*left* hemisphere with even gray level), the vegetal pole (*right* hemisphere with granular appearance), and the nucleus within the animal pole (see the magnified and filtered *inset*). The edge enhancement is extremely clear for the outer boundary of the oocyte and also visible for the boundary between the nucleus and the surrounding region (*inset*).

The different appearance of the left and right hemisphere can be attributed to an inhomogeneous distribution of cytoskeletons creating an asymmetry between the two hemispheres. The animal pole has much more densely connected keratin than the vegetal pole (Gard et al., 1997). The mesh size is 10 μm in the vegetal pole, 10 times larger than those in the animal pole. The much smaller mesh size of the cytoskeleton network and the presence of pigment granules ($\sim$1 μm in diameter) blur the edges of the network and only an evenly distributed gray level is observed in the animal pole.

These arguments are consistent with the electron microscopy results (Gard et al., 1997). In addition, our technique leads to nondestructive and three-dimensional (3D) observation of the oocyte interior. Also note that the observation of the nucleus within the animal pole is important because it could lead to the observation of the embryogenesis of vertebrates in real time, which is not possible with optical microscopy due to opacity.

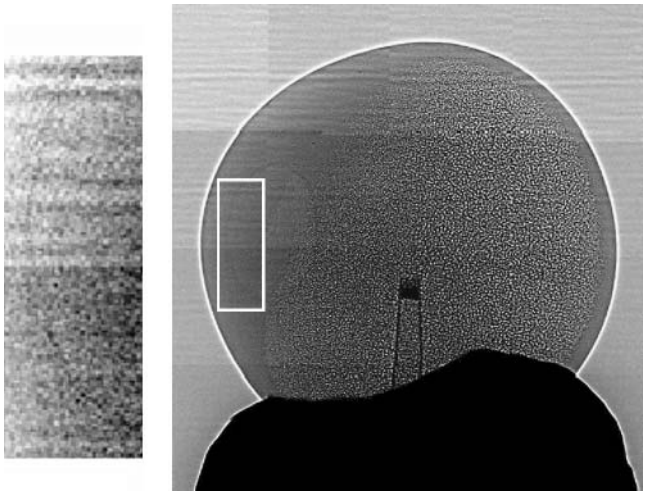

FIGURE 1 Phase-contrast micrograph showing the interiors of a *Xenopus* oocyte. A sharp-tipped glass capillary (visible in the *middle* of the image) was used to fix the sample to the holder (the *bottom* dark region). The sample diameter was 1.5 mm. The inset shows a magnified version of the marked left-hand portion of the image. This magnified picture was processed to emphasize the boundary of the nucleus.

MATERIALS AND METHODS

Instrumentation

The tests were performed with a microradiography system whose details are described in Baik et al. (2004). Unmonochromatized x-ray beams from the 7B2 beamline of the Pohang Light Source and the PCI beamline of the Singapore Synchrotron Light Source were used to illuminate the sample. The transmitted x rays were captured by a cleaved $CdWO_4$ single-crystal scintillator and converted to a visible image. This image was then magnified by an optical lens before being captured and stored by a charge-coupled device camera.

The samples were mounted on a translation/rotation stage that allowed precise positioning. For biological samples with intrinsically limited x-ray absorption, a single image (typically 1280 $\times$ 1024 pixel, horizontal field of view (FOV) 500 μm) could be taken within 100 ms. The corresponding radiation dose did not produce any detectable damage.

Sample preparation

The leaf cell samples were obtained from *Hippeastrum epidermis*. Tissue specimens were obtained by peeling off the bottom skin of the leaf and then sandwiched between two moisturized Kapton foils to preserve water. The thickness of the leaf skin is $\sim$30–50 μm and the Kapton foil is 50 μm. Such a procedure was not required to observe cells; it was possible to see individual cells even in the leaf without peeling. The peeling and sandwiching procedure, however, eliminated a problem: the superposition of many cell layers results in complicated images. An alternate solution for this problem is tomography. We demonstrated the tomography reconstruction of plant cell by using thick samples ($\sim$5 mm) taken from the skin part of an aloe leaf.

Oocytes were selected for our tests to assess the penetration and the spatial resolution of our approach. Oocytes at stage 6 were surgically removed from the ovary of a *Xenopus* and incubated at 18°C in the standard ND96 medium (in mM) (NaCl, 96; KCl, 2.0; $CaCl_2$, 1.8; $MgCl_2$, 1.0; and HEPES, 5, pH 7.6).

Cerebral neurons from rat brains were prepared from an 18-day-old rat embryo (Lin et al., 2002). They were placed on a coverslip glass locally coated with poly-D-lysine so that neurons accumulated over the poly-D-lysine patches. Cell cultures were incubated at 37°C with 95% humidity and 5% CO_2. The samples for the microradiology tests were prepared from the culture after 9–11 days of incubation. A medium with collagen was used to seal the neurons on the coverslip and a gel-like layer was formed after $\sim$20 min in ambient air at room temperature. The average thickness of the samples was $\sim$200 μm.

Fibroblast cells were used to test the feasibility of detecting changes in the cell morphology. The cell line (HIG-82) was obtained from the Food Science Research Institute (Industrial Technology Research Institute, Taiwan). It was prepared from the fibroblast of rabbit joints. The cells were cultured in 35-mm culture dishes without specific coating at the bottom and incubated at 37°C with 95% humidity and 5% CO_2. The medium was Ham's F-12 medium (2 mM L-glutamine and Earle's buffered salt solution adjusted to contain 1.5 g/L sodium bicarbonate, 0.1 mM nonessential amino acids, and 1.0 mM sodium pyruvate 90%; fetal calf serum, 10%). Dishes with $\sim$80% cell confluence were prepared for microradiology tests after fixation.

All animal cell samples were fixed with 4% paraformaldehyde overnight before being mounted on the sample holder. The oocyte was placed in air. The coverslips with the neurons were placed in a sealed plastic bag to preserve sufficient moisture. The HIG-82 fibroblast cells were observed with

the culture dish water-tight sealed and vertically placed in the path of the x-ray beam.

For preparation of mouse aorta, adult C57/BL6 mice were anesthetized with ether inhalation and were perfusion fixed via direct intracardiac injection, initially with heparinized PBS (10 units/ml) followed by phosphate-buffered 2% paraformaldehyde (pH 7.4) for 10 min (Yeh et al., 2003). The thoracic aortas were dissected and cut into transverse rings. Thereafter the aortas were embedded in resin using standard preparation procedures for thin-section electron microscopy (Blackburn et al., 1995).

The above-described preparation procedures are much less complicated than the standard methods for optical microscopy and other microscopy techniques—and resulted in specimens very close to their natural state. Specifically, no staining or other contrast-enhancing procedure was used. The cultured cells were fixed to preserve their morphology because the x-ray beam propagates horizontally and therefore the specimens had to be placed vertically. The specimens were much thicker than for optical microscopy and an opaque medium could be used.

RESULTS AND DISCUSSION

The specific objectives of our tests were the following. First, we wanted to demonstrate sufficient (submicron) lateral resolution and contrast with hard x rays (wavelength <0.1 nm) to detect cellular details. Second, we wanted to show such a performance with thick samples and without complicated sample processing. Third, we sought specific evidence of cellular-level imaging of live specimens. The fourth objective was detection in real time on a video ($\approx$33 ms) timescale.

All such objectives were reached with tests on the already-mentioned variety of specimens. Figs. 2 and 3 show microradiographs of a *Hippeastrum* leaf taken with broadband (unmonochromatized) x rays. The (horizontal) FOV was $\sim$1.5 mm.

These images constitute, to the best of our knowledge, the very first example of cell radiographs obtained with hard x rays without staining. Fig. 2 shows the leaf skin (thickness $\sim$30–50 μm) whereas Fig. 3 shows the entire leaf (thickness $\sim$300 μm). The little triangle-shaped features in Fig. 3 are the gaps among the spongy parenchyma cells under the palisade cells. Note that x ray can penetrate into the leaf and reveal the different morphologies of these cells and their packing. Fig. 3 stresses the difference with respect to optical microscopy: not only cells in the outermost layer are visible but also deeper cells.

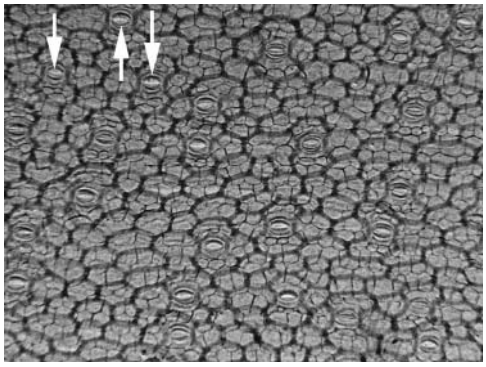

FIGURE 2 Microradiograph of a *Hippeastrum* leaf taken with broadband (unmonochromatized) x rays. The image size was 1.5 $\times$ 1 mm. The figure shows cells from the leaf skin membrane. The arrows identify three of the stoma cells. To the best of our knowledge, these results constitute the first example of cell radiographs without staining.

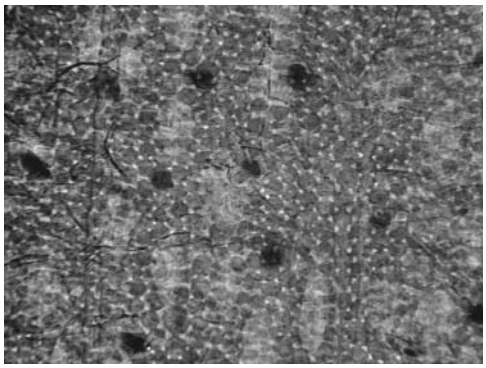

FIGURE 3 Microradiograph showing the entire leaf depth.

The arrows in Fig. 2 identify stomata in the epidermis as they open up. Such cells enabled us to demonstrate real-time imaging of live specimens. Fig. 4 shows in fact individual images captured from a movie taken with a video camera. The images clearly show the opening of a live stoma cell.

A careful examination of the sequence of images in Fig. 4 reveals features beyond the mere opening. These include subcellular features and the induced changes (such as compression and displacement) of the surrounding cells. We suspect, for example, that the darker lines on the guard cells are those from the cellulose microfibrils. The live detection of such minute movements is quite remarkable if one considers the complete absence of staining.

We also tested a procedure to enhance the moving cell with respect to the nonmoving ones by subtraction. This is quite desirable because the nonmoving cells inside the leaf (particularly the parenchyma cells) have much stronger contrast than the epidermal cells and outer cuticle and therefore complicate the image when one tries to observe the movement in a natural, unpeeled leaf. The first tests are encouraging and may provide a simple and feasible alternate procedure with respect to tomography.

In parallel, we performed successful tests of tomographic reconstruction of microradiographs of plants cells. We used a standard filtered back projection algorithm from 1000 projections. We found that the boundaries of individual cell can be effectively reconstructed. Fig. 5 shows an example of reconstruction performed for the skin of an aloe leaf $\sim$5-mm thick. Note that only the area near the surface (shown in Fig. 5) is reconstructed due to the limited field of view whereas the entire thick sample was kept during the image acquisition for the required tomography reconstruction. The quality of the reconstruction was not optimized due to the slight movement of the sample during the measurements. Moreover,

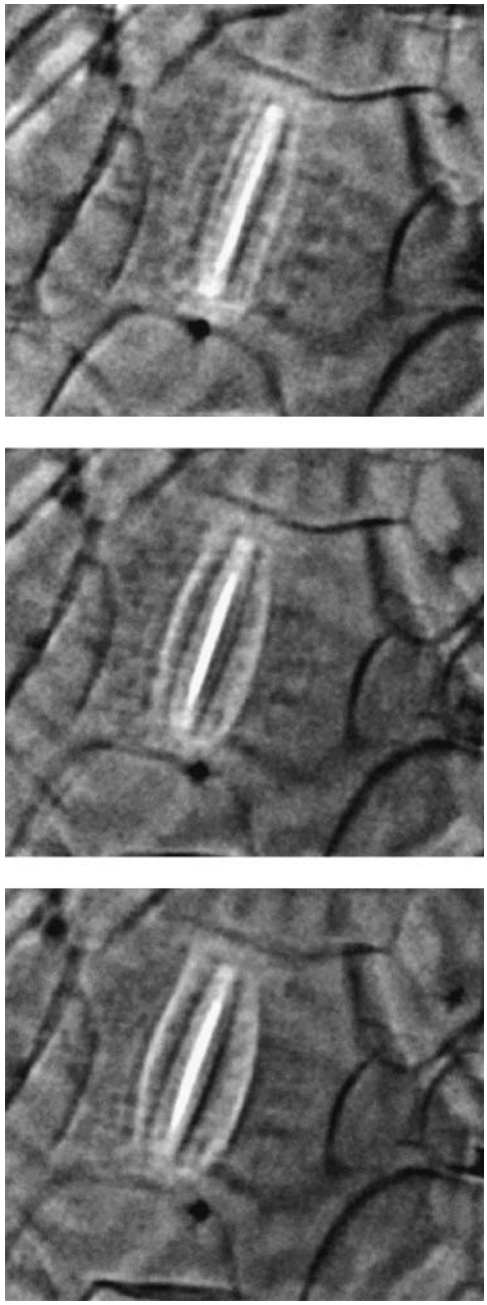

FIGURE 4 Images captured from a movie taken with a video camera showing the opening movement of a live stoma cell.

although the image sequence was taken within 2 min, notable dehydration was observed. The reconstruction was also blurred by the ''local tomography'' effects (Faridani et al., 1997; Anastasio et al., 2003) due to the large dimension of the sample, which is larger than the field of view of each individual projection. In this specific case, the dimension of the sample was $5 \times 5 \times 5$ mm but only $\sim 400 \times 400 \times 300$ μm was reconstructed. The corresponding artifacts are most noticeable in the area away from the center of rotation. Such problems notwithstanding, the tests clearly show that tomographic reconstruction is feasible for thick samples.

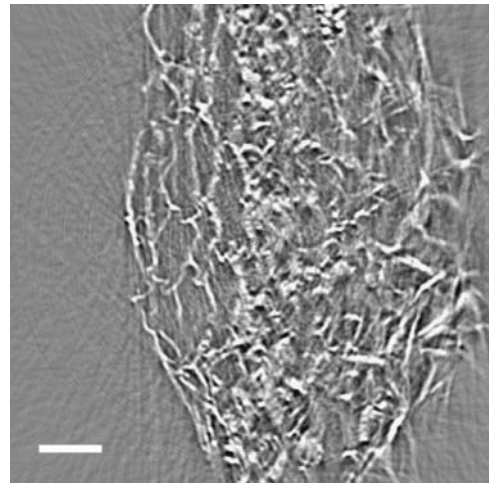

FIGURE 5 Tomographic reconstruction of an aloe leaf sample. The reconstruction is based on 1000 projections taken within 2 min. Scale bar is 50 μm.

To better demonstrate this high ''selectivity'' resulting from the enhanced contrast due to phase effect and from the high-penetration nature of x rays, we show in Fig. 6 a similar local tomography reconstruction of a toothpick. The diameter of the toothpick is $\sim$3 mm and the reconstructed area is 240×240 μm. The quality of the reconstructed image is improved with respect to the previous case by the elimination of the artifacts due to dehydration-induced sample movement as seen for the aloe leaf. In the inset, it is clear that small features can still be easily detected despite the rather large sample examined. Fig. 6 *b* shows the 3D volume-generated surface contour image constructed from the tomography reconstructed data as exampled in Fig. 6 *a*. Note that not only each channel is clear imaged, but also the texture of the cell walls along the direction parallel to the rotation axis.

The added phase effect, however, complicated the tomography reconstruction based on the filtered back projection algorithm. One can use a more rigorous approach to extract the embedded phase information (Bronnikov, 2002; Barty et al., 2000; Cloetens et al., 2002) and obtain the real-space image before initiating the normal tomography reconstruction. Another simpler approach is to consider the phase effects, in this case the dark and bright fringes on the edge, simply as a region of light adsorption. By adjusting the sample to detector distance, such phase effect can be optimized for best visual clarity without adding unwanted effect to the tomography reconstruction as demonstrated in the previous examples.

Note that in conventional tomography the reconstruction based on absorption works because absorption follows a linear dependence along the line of projection. This is in fact a consequence of the small magnitude of the imaginary

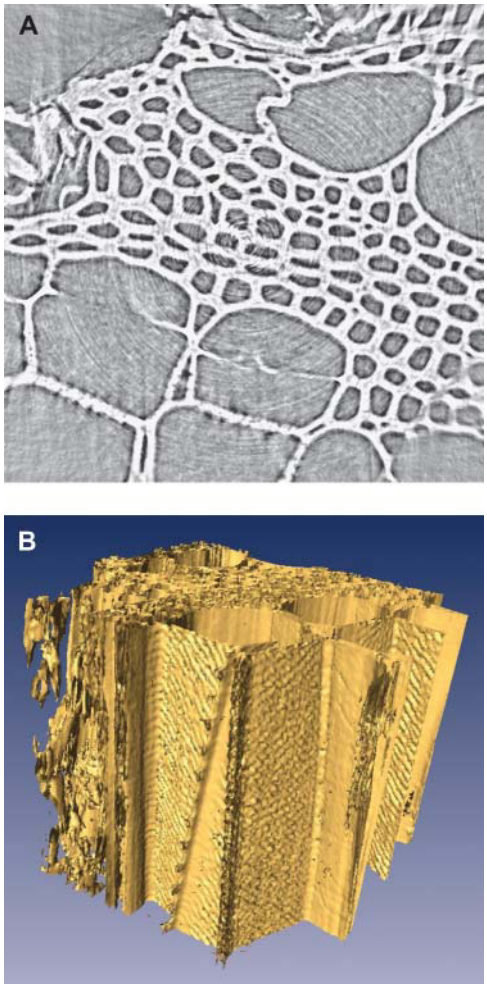

FIGURE 6 (*a*) Tomographic reconstruction of a toothpick, used to assess the resolution performances of our apparatus and procedure. The diameter of the sample is ~3 mm but only a central area of diameter ~240 μm is reconstructed. Features of μm size can be observed. (*b*) The volume-rendered 3D structure of the same toothpick sample.

part of the refractive index. Similarly, the phase shift due to the real part of the refractive index is approximately linear, because the real part is very close to unity and the imaginary exponential in the wave function leads to a constant-phase factor multiplied by a linearly changing phase factor.

Plant cells are quite easy to image with our approach. Figs. 7 and 8, however, show that animal cells can be seen as well. Fig. 7 shows cultured and fixed neuron cells from mouse brain. Not only are the neuron bodies clearly visible but also the interconnected axons.

Specifically, it is possible to observe the region under the ganglion neurons so that the attachment of the neurons with the extracellular matrix and with one another can be revealed. The x-ray penetration to the region under the ganglion surface could be exploited to analyze neurons-glia interactions and even the interaction between cells and bones.

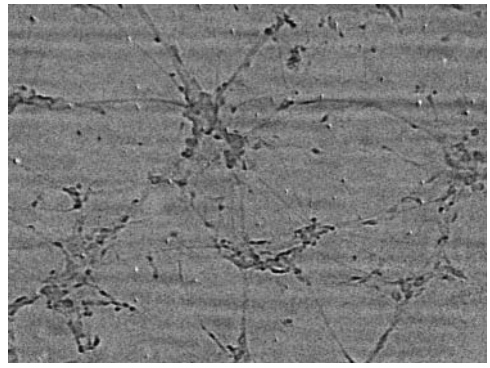

FIGURE 7 Radiograph of cultured and fixed neuron cells from mouse brain. The field of view (horizontal) was 500 μm.

Note that the neuron specimens were not even optimized for x-ray imaging. In fact, the collagen used for sealing was obtained from three rat tails and dissolved in 0.1% acetate at the concentration of 2 mg/ml, which is not specially designed for microradiology and therefore leads to weak contrast. The fixation collagen are also quite thick, ~300 μm, much more than normally required for optical microscopy. The slight blurring in the microradiographs is likely due to collagen-induced diffuse scattering and can be improved by further optimization of the collagen materials.

Fig. 8 shows cultured fibroblast cells from rabbit joints. The cells can be fixed with paraformaldehyde before mounting the specimen in a vertical position. The fixed cells were then tightly packed and all with a fibril or spindle shape. In contrast, Fig. 8 shows the same type of cells imaged without being fixed: the cells are not close packed and morphological modifications can be seen. Nevertheless, the image quality is still quite reasonable, indicating that our approach can be used for mammalian cells in their natural state.

With suitable fixation procedures, we could even obtain high-resolution tomography and 3D reconstructed images of mammalian cells. Fig. 9 *a* shows an example. The sample is

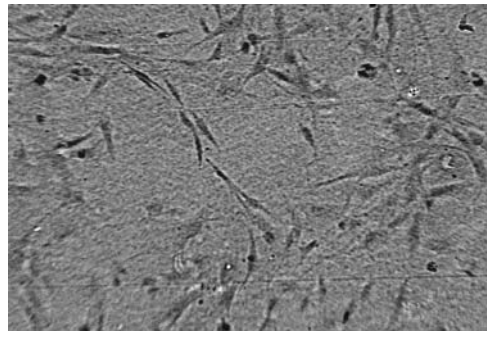

FIGURE 8 Radiograph of cultured fibroblast cells extracted from a rabbit bone. The cell samples were again vertically mounted but not fixed. The field of view (horizontal) was 500 μm.

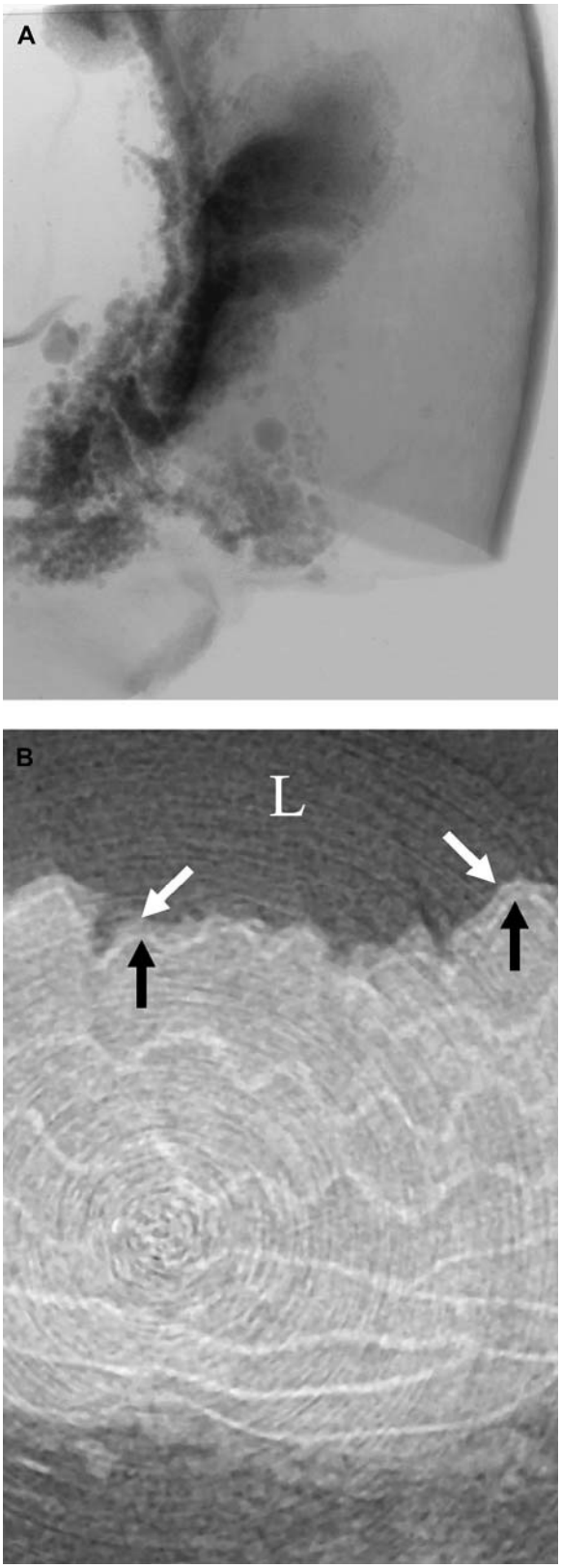

FIGURE 9 (*a*) X-ray micrographs of a mouse aorta sample fixed in resin; the overall sample dimension, including the resin, is ~5 × 7 × 10 mm. Scale bar is 400 μm. (*b*) One of the tomography reconstructed slices. The detailed structure of the vessel wall is clearly seen even if the sample is larger than the imaged area. The aorta wall is layered by the waving elastic laminae, the innermost of which, internal elastic lamina (marked by *black arrows*), is isolated from the lumen (*L*) by a monolayer of endothelial cells (*white arrows*). Scale bar is 15 μm.

a piece of aorta fixed in resin; the overall sample dimension, including the resin, is ~5 × 7 × 10 mm. Fig. 9 *b* shows one of the tomography reconstructed slices. In this cross-sectional view of mouse aorta, ~240- × 240-μm field of view, the detailed structure of the vessel wall is clearly observed after tomography reconstruction despite the fact that the sample is larger than the imaged area. The aorta wall is layered by the waving elastic laminae, the innermost of which, the internal elastic lamina (marked by *black arrows*), is isolated from the lumen (*L*) by a monolayer of endothelial cells (*white arrows*). Fig. 10 is the volume-rendered 3D structure of this sample. The white arrows point to borders between neighboring cells, whereas the black arrow points to a cell nucleus that extrudes from the surface and whose outline is well preserved in the 3D reconstruction analysis. In this case, the imaging capability goes beyond the mere imaging of the outline and shape of the individual cell and provides subcell information.

Our results, thus, show that refractive index imaging based on coherent x rays can produce clear images at the cell and sometimes subcell level without staining. It is quite important to compare this approach to other techniques and assess its advantages, limitations, and possible future improvements. The resolution obtained so far is similar to optical microscopy and can be substantially improved. Soft x-ray microscopy has better resolution but has not been implemented on samples thicker than a single layer of cells. Transmission electron microscopy and scanning electron microscopy require specific sample preparation procedures and are limited in the sample thickness. Overall the biggest advantage of our approach is offered by the high penetration of hard x rays, easily the whole body of an animal, and the consequent potential to examine systems close to natural living conditions. No microscopy in fact matches refractive index microradiology in examining thick and opaque specimens with high resolution (W. Yun, private communication).

This approach is certainly not without limitations. The possible radiation damage is certainly less severe than in absorption-contrast radiology but it cannot be neglected. In most of the two-dimensional measurements, where exposure to synchrotron x rays can be limited, radiation damage or dehydration is not observed. Although not evident in our tests, this issue must nevertheless be carefully explored to assess its impact. The longer data-taking time required for the tomography (sometimes >1000 snapshots at different angles is necessary to preserve the resolution) could aggravate the problem. On the other hand, the current time per frame (1 ms) (Hwu et al., 2004) and the corresponding dose

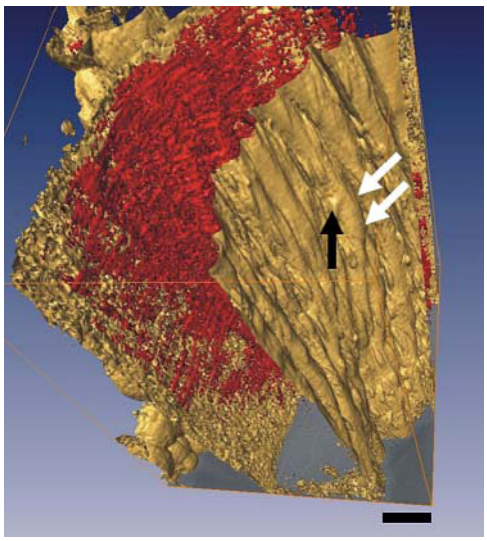

FIGURE 10 The volume-rendered 3D structure of the same aorta sample of Fig. 9. The white arrows point to borders between neighboring cells, whereas black arrow points a cell nucleus that extrudes from the surface and whose outline is well preserved in the 3D reconstruction. Scale bar is 50 μm.

can be reduced by 1–2 orders of magnitude with advanced detectors.

As to other future improvements, the full development of tomographic reconstruction will further exploit the key advantage of our approach in exploring thick living samples up to a few mm with minimal sample preparation. The technique will be further enhanced by the future ultrabright x-ray laser and by the potential to implement new image detection strategies with their ultrashort pulses.

CONCLUSIONS

The limited absorption by biological tissues has so far prevented x rays from producing radiological images of individual cells without staining. We demonstrated that this limitation can be overcome. We specifically presented hard-x-ray radiographs of different types of living and nonliving cells with no staining at all.

The result was achieved by using coherent x rays from a synchrotron source with no monochromatization (because very limited longitudinal coherence was required) (Hwu et al., 2002; Margaritondo, 2002), x-ray detection with high lateral resolution, and a detection geometry that enhances the contrast due to variations in the x-ray refractive index. The image quality in these first tests is not yet at the same level as state-of-the-art optical microscopy. However, there is substantial potential for quality improvement, and, of course, x-ray images have the strong advantage of revealing internal features of a large specimen in a rather natural environment.

Several aspects of our tests should be further explored. For example, possible radiation damage, not observed in our first tests, should be systematically explored. Although our technique can already clearly detect different cell morphologies and cell details, even finer internal structure details should become visible at higher magnification. Furthermore, future x-ray lasers will provide ultraintense and ultrashort pulses to perform one-shot imaging before damage. Even without waiting for these future developments, our tests clearly show that coherent microradiology is a very helpful instrument in cell biology, largely complementary to optical microscopy.

We are grateful to W. Y. Chow and Y. C. Chang (Department of Life Science, National Tsing Hua University, Taiwan) for providing oocytes and neurons for our experiments.

This work was supported by the National Science Council (Taiwan), the Academia Sinica (Taiwan), the BK21 Project, the Korea Institute of Science and Technology Evaluation and Planning through the National Research Laboratory and SKORE-A projects, the Fonds National Suisse de la Recherche Scientifique, the Ecole Polytechnique Fédérale de Lausanne, and the National University of Singapore.

REFERENCES

Anastasio, M. A., F. De Carlo, and X. Pan. 2003. Phase-contrast tomography and the local tomography problem. *Proc. SPIE.* 5030: 120–126.

Baik, S., H. S. Kim, M. H. Jeong, C. L. Lee, J. H. Je, Y. Hwu, and G. Margaritondo. 2004. International consortium on phase contrast imaging and radiology beamline at the Pohang Light Source. *Rev. Sci. Instrum.* 75:4355–4358.

Barty, A., K. A. Nugent, A. Roberts, and D. Paganin. 2000. Quantitative phase tomography. *Opt. Commun.* 175:329–36

Blackburn, J. P., N. S. Peters, H. I. Yeh, S. Rothery, C. R. Green, and N. J. Severs. 1995. Upregulation of connexin43 gap junctions during early stages of human coronary atherosclerosis. *Arterioscler. Thromb. Vasc. Biol.* 15:1219–1228.

Bronnikov, A. 2002. Theory of quantitative phase-contrast computed tomography. *J. Opt. Soc. Am. A.* 19:472–480.

Cloetens, P., W. Ludwig, E. Boller, L. Helfen, L. Salvo, R. Mache, and M. Schlenker. 2002. Quantitative phase-contrast tomography using coherent synchrotron radiation. *Proc. SPIE.* 4503:82–91.

Faridani, A., D. Finch, E. L. Ritman, and K. T. Smith. 1997. Local tomography II. *SIAM J. Appl. Math.* 57:1095–1127.

Ford, T., W. Meyer-Ilse, and A. D. Stead. 2000. Development and evaluation of cryo-imaging of unicellular algae using soft X-ray transmission microscopy: ultrastructure and elemental analysis. W. Meyer-Ilse, T. Warwick, and D. Attwood, editors. *Proc. of the 6th X-Ray Microscopy Conference, American Institute of Physics, College Park, MD.* 507:119–122.

Gard, D. L., B. J. Cha, and E. King. 1997. The organization and animal-vegetal asymmetry of cytokeratin filaments in stage VI *Xenopus* oocytes is dependent upon F-actin and microtubules. *Dev. Biol.* 184:95–114.

Hwu, Y., W.-L. Tsai, A. Groso, G. Margaritondo, and J. H. Je. 2002. Coherence-enhanced synchrotron radiology: simple theory and practical applications. *J. Appl. D: Appl. Phys.* 35:R105–R120.

Hwu, Y., W. L. Tsai, J. H. Je, S. K. Seol, B. Kim, A. Groso, G. Margaritondo, K.-H. Lee, and J.-K. Seong. 2004. Synchrotron micro-angiography with no contrast agent. *Phys. Med. Biol.* 49:501–508.

Kirz, J., H. Ade, E. Anderson, C. Buckley, H. Chapman, M. Howells, C. Jacobsen, C. H. Ko, S. Lindaas, D. Sayre, S. Williams, S. Wirick, and X. Zhang. 1994. New results in soft X-ray microscopy. *Nucl. Instrum. Methods.* B87:92–97.

Jacobsen, C., T. Beetz, M. Feser, A. Osanna, A. Stein, and S. Wirick. 2002. Spectromicroscopy of biological and environmental systems at Stony Brook: instrumentation and analysis. *Surf. Rev. Lett.* 9:185–191.

Larabell, C. A., D. Yager, and W. Meyer-Ilse. 2000. Localization of proteins and nucleic acids using soft X-ray microscopy. W. Meyer-Ilse, T. Warwick, and D. Attwood, editors. *Proc. of the 6th X-Ray Microscopy Conference*, *American Institute of Physics*, *College Park*, *MD*. 507:107–112.

Lin, Y. C., Z. H. Huang, I. S. Jan, C. C. Yeh, H. J. Wu, Y. C. Chou, and Y. C. Chang. 2002. Development of excitatory synapses in cultured neurons dissociated from the cortices of rat embryos and rat pups at birth. *J. Neurosci. Res.* 67:484–493.

Margaritondo, G. 2002. Elements of Synchrotron Light for Biology, Chemistry, and Medical Research. Oxford University Press, New York.

Miao, J. W., T. Ishikawa, B. Johnson, E. H. Anderson, B. Lai, and K. O. Hodgson. 2002. High resolution 3D X-ray diffraction microscopy. *Phys. Rev. Lett.* 89:088303.

Weiß, D., G. Schneider, B. Niemann, P. Guttmann, D. Rudolph, and G. Schmahl. 2000. Tomographic imaging of cryogenic biological specimens with the X-ray microscope at BESSY I. W. Meyer-Ilse, T. Warwick, and D. Attwood, editors. *Proc. of the 6th X-Ray Microscopy Conference*, *American Institute of Physics*, *College Park*, *MD*. 507:123–128.

Yeh, H.-I., C.-S. Lu, Y.-J. Wu, C.-C. Chen, R.-C. Hong, Y.-S. Ko, M.-S. Shiao, N. J. Severs, and C.-H. Tsai. 2003. Reduced expression of endothelial connexin37 and connexin40 in hyperlipidemic mice: recovery of connexin37 after 7-day simvastatin treatment. *Arterioscler. Thromb. Vasc. Biol.* 23:1391–1397.

Yun, W. 2004. [online]. http://www.xradia.com.

Yun, W., B. Lai, A. Krasnoperova, E. Di Fabrizio, Z. Cai, F. Cerrina, Z. Chen, M. Gentili, and E. Gluskin. 1999. Development of zone plates with a blazed profile for hard x-ray applications. *Rev. Sci. Instrum.* 70: 3537–3541.